Networked UAV Detection and Alerting of Ionospheric Anomalies within LADGNSS Navigation Framework

Gihun Nam, K. Andrew Sun, and Jiyun Lee, *Korea Advanced Institute of Science and Technology*
Sam Pullen, *Stanford University*

Abstract

Local Area Differential GNSS (LADGNSS) is a simplification of the Ground-based Augmentation System (GBAS) architecture to provide navigation and guidance for nearby UAVs. Recent research has evaluated the impacts of severe ionospheric anomalies on Dual-Frequency, Multiple-Constellation (DFDC) LADGNSS and its monitors. To protect against all possible ionospheric anomalies, the system assumes that the worst-case undetected ionosphere-induced differential errors might affect users. The hypothetical impact of ionospheric anomalies can be lowered by improving monitoring capability, and one possible improvement not studied previously is to utilize two-way transmissions from the multiple networked UAVs supported by LADGNSS at any given time. Two-way datalinks are already part of the LADGNSS architecture to support UAV status reports and cooperative guidance, and they can be exploited to allow all UAVs connected to LADGNSS ground stations to share the threat information collected by any of them.

This paper examines the benefit of networked UAVs for LADGNSS under anomalous ionospheric conditions by proposing a monitor strategy that leverages observations from networked UAVs to enhance ionospheric monitor capability. The strategy utilizes UAVs within the network which have superior ionospheric gradient monitor (IGM) detection capability to reduce the maximum undetected gradient of a specific user UAV, leading to reduced maximum undetected ionosphere-induced differential errors (MIEV) at that user. Simulation results show a significant reduction in the worst ionosphere-induced differential error by utilizing multiple monitor capability of networked UAVs, where the benefit increases with a larger number of UAVs that are more widely distributed.

1. INTRODUCTION

In previous research, the use of a simplified Local Area Differential GNSS (LADGNSS) architecture to provide navigation and guidance to nearby Unmanned Aerial Vehicles (UAVs) has been explored (e.g., see Pullen et al., 2013, Kim et al., 2017). LADGNSS ground stations would provide integrity based on the Ground-based Augmentation System (GBAS) architecture but with lower-cost equipment with greatly reduced siting constraints. The objective is to provide both decimeter-level 95% accuracy and position-domain protection levels of several meters to a probability of $1 - 10^{-7}$ per operation while mitigating the same threats as GBAS. The LADGNSS ground system and its datalink would be coupled with the command and guidance system that directs each UAV and coordinates UAV operations within 25 – 50 km of each installation.

Recent work on LADGNSS for UAVs has examined the threat of anomalous ionospheric spatial decorrelation, which is a major concern for GBAS. In Nam et al., (2022), modifications to monitors proposed for future dual-frequency, multi-constellation (DFMC) GBAS were evaluated, showing that worst-case undetected errors for LADGNSS can be limited to below 5 meters. However, monitors developed for GBAS are limited by the one-way nature of the GBAS VHF Data Broadcast (VDB) from ground station to aircraft. In contrast, LADGNSS supports two-way transmissions to facilitate UAV guidance and real-time status reporting. This feature also supports navigation integrity by relaying relevant UAV monitor statistics and protection levels back to the ground station.

This paper examines the use of UAV-to-ground-station transmissions from a "networked" configuration of UAVs (meaning, in this case, all UAVs are continuously connected to the LADGNSS ground station but not necessarily to each other) by proposing a monitor strategy that leverages UAV observations to enhance detection of anomalous ionospheric threats. This allows the LADGNSS ground system to utilize the monitor with the best detection capability among all UAVs within its coverage. The benefit of what we call

"networked ionospheric monitoring" varies with the configuration of the supporting UAVs. Therefore, this paper also evaluates the impact of worst-case ionospheric anomalies based on varying arrangements of UAVs (idealized and randomized) and finds the configuration from which the optimal benefit from networked monitoring can be obtained.

Section 2 of this paper explains the detection capability of the dual-frequency ionospheric gradient monitor (IGM) which depends on distance between the reference station and each UAV that implements this monitor. Section 3 describes the networked ionospheric monitoring algorithm which enables ground station use of all IGM test statistics, including the one with the best detection capability among the networked UAVs. Section 4 presents the results of simulations of the networked monitoring procedure for randomly and ideally distributed configurations of UAVs to evaluate the benefit of the networked monitoring. Specifically, worst-case ionosphere-induced vertical position errors (MIEVs) and protection levels (PLs) are shown for different configurations of networked UAVs. Section 5 summarizes the paper.

2. DETECTION CAPABILITY OF IONOSPHERIC GRADIENT MONITOR (IGM)

The DFMC LADGNSS system presented in previous work (Nam et al., 2021, Nam et al., 2022) utilizes the ground/airborne code-carrier divergence (CCD) monitors and dual-frequency IGM for detecting anomalous ionospheric gradients. This study utilizes dual-frequency IGM (Felux, 2018) for networked ionospheric monitoring because its detection capability depends on ionospheric pierce point (IPP) geometry of both ground station and airborne receivers; therefore, the detection capability of the networked monitor can be easily determined for a given configuration of networked UAVs.

Dual-frequency IGM directly compares ground and airborne ionospheric estimates for each satellite to detect the anomalous ionospheric gradient between the ground station and an observing user (Felux, 2018). The test statistic of dual-frequency IGM is defined as the differential ionospheric delay estimate ($\tilde{I}_{test,n}$) for the nth satellite:

$$\tilde{I}_{test,n} = \tilde{I}_{gnd,n} + \tilde{I}_{air,n} \tag{1}$$

where the expression of the ground ($\tilde{I}_{gnd,n}$) and airborne ionospheric estimates ($\tilde{I}_{air,n}$), and the unbiased expression of the test statistics ($I_{test,n}$) are presented in Nam et al., (2022).

The minimum detectable differential ionospheric delay (MDID) of IGM then can be expressed as follows:

$$MDID_n = (k_{ffa} + k_{md})\sigma_{test,n} \tag{2}$$

where k_{ffa} is the multiplier satisfying the sub-allocated fault-free detection requirement and k_{md} is the multiplier satisfying the sub-allocated missed detection requirement. The standard deviation of the test statistic ($\sigma_{test,n}$) can be expressed as follows (Nam et al., 2022):

$$\sigma_{test,n} = \sqrt{\sigma_{iono,n}^2 + \left(\frac{f_x^2}{f_x^2 - f_y^2}\right)^2 \left(\sigma_{gnd,n}^2 + \sigma_{air,n}^2\right)} \tag{3}$$

where $\sigma_{iono,n}$ is the standard deviation of the ionospheric decorrelation, and $\sigma_{gnd,n}$ and $\sigma_{air,n}$ are the standard deviations of ground and airborne multipath and thermal noise for the nth satellite, respectively. This study assumes the use of a dual-frequency divergence free smoothing method to directly measure the ionospheric delay difference (i.e. test statistics of IGM), which does not include the synthetic separation effect from the smoothing filter.

Figure 1 (left) presents a differential range error between the ground station and the user where the ionospheric front for a given direction spans over the ground and user IPPs. The LADGNSS users assume that the worst possible ionospheric gradient (g_{max}) always presents and their differential range measurement can be corrupted by the largest ionosphere-induced error, $g_{max} \cdot x_{user}$ where

x_{user} is a distance from IPP of the ground station to that of the user. The IGM of the user can reliably detect an ionospheric gradient which causes the differential range error larger than the MDID of the IGM. Therefore, the user can detect the anomaly whose gradient is greater than the maximum undetected gradient ($g_{max,user}$) of the user which is expressed as follows:

$$g_{\max,user} = MDID_{user} / x_{user} \tag{4}$$

As a result, the worst ionosphere-induced range error with the IGM is the MDID of the user's IGM, which can be also expressed as $g_{max,user} \cdot x_{user}$ as given in Figure 1 (left).

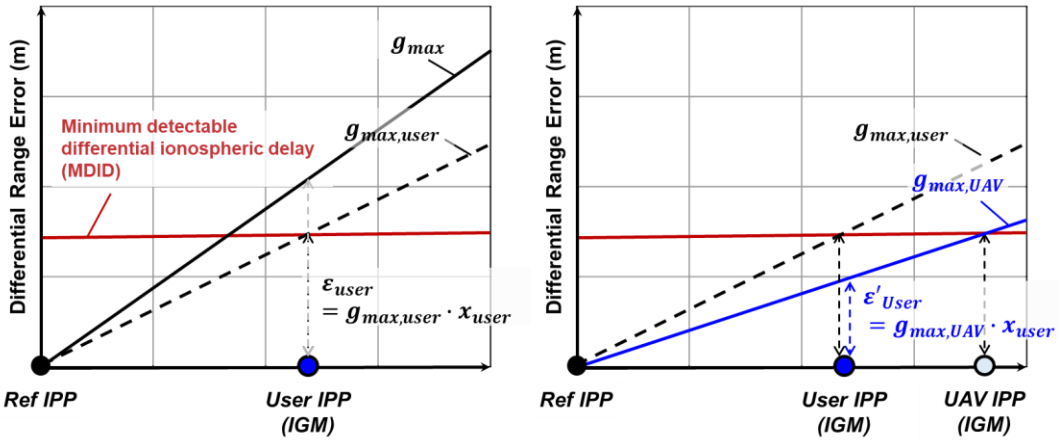

Figure 1 *The differential range errors of the user under the worst undetected gradients with and without the IGM of the user (Left) and with the IGM of the UAV located farther from the reference station (Right). The MDID of IGM (denoted as the red solid curve) varies as a function of the distance from the reference station.*

If an additional UAV is located farther from the ground station as shown in Figure 1 (right), the "farther UAV" experiences larger ionosphere-induced delay differential errors for the same ionospheric gradient, $g_{max,user}$, while the MDID of IGM barely increases along the distance from the reference station. Therefore, the IGM of the UAV farther from the ground station has a higher detection capability than the IGM of the user. The IGM of the farther UAV can detect ionospheric gradients larger than $g_{max,UAV}$, which is lower than $g_{max,user}$, expressed as follows:

$$g_{\max,UAV} = MDID_{UAV} / x_{UAV} \tag{5}$$

In this case, the worst ionosphere-induced range error for the user in the presence of the farther UAV is $g_{max,UAV} \cdot x_{user}$ as given in Figure 1 (right).

3. NETWORKED IONOSPHERIC MONITORING ALGORITHM

As explained in Section 2, UAVs located farther from the ground station have a better detection capability of IGM than UAVs located inside, when all IPPs for a given satellite are impacted by the same ionospheric front. This indicates that the inner UAVs can take advantage of the higher detection capability of any outer UAV's IGM by sharing their monitor status via the ground station. Here we present a generalized algorithm for the "networked ionospheric monitoring" which takes advantage of the best detection capability among all IGMs of networked UAVs, for all possible direction of ionospheric anomalies.

Figure 2 (left) shows an IPP configuration of the ground station and a single UAV when the direction of ionospheric front is fixed to $\theta°$ from the east vector. In this case, the maximum undetected gradient for the UAV 1 on a fixed anomaly direction of $\theta°$ can be computed as follows:

$$g_{\max,UAV_1}(\theta) = MDID_{UAV_1} \Big/ (\vec{d}_{GF,UAV_1} \cdot \hat{b}_\theta) \tag{6}$$

where $\vec{d}_{GF,UAV_1}$ is a vector from the ground station to the UAV_1 and $\hat{b}_\theta$ is a unit vector with the angle θ° from the east vector; therefore $\vec{d}_{GF,UAV_1} \cdot \hat{b}_\theta$ is a projected distance from the ground station to the UAV_1 on the direction of anomaly θ° as shown in Figure 2 (left). If we extend this algorithm to multiple UAVs as shown in Figure 2 (right), we can choose the UAV with the best detection capability which has the minimum value of the maximum undetected gradient among all UAVs. Then the general expression of the maximum undetected gradient of networked UAVs ($g_{max,net}$) can be obtained by searching for all possible direction of anomaly as follows:

$$g_{\max,net} = \max_{0 \le \theta < 2\pi} \min_{i \subset N} g_{\max,UAV_i}(\theta) \tag{7}$$

where N is the number of UAVs in a given network. In this study, we set the upper bound of the maximum gradient as 425 mm/km, which is the maximum bound of ionospheric gradients defined in the CONUS ionospheric threat model (Datta-Barua et al., 2010).

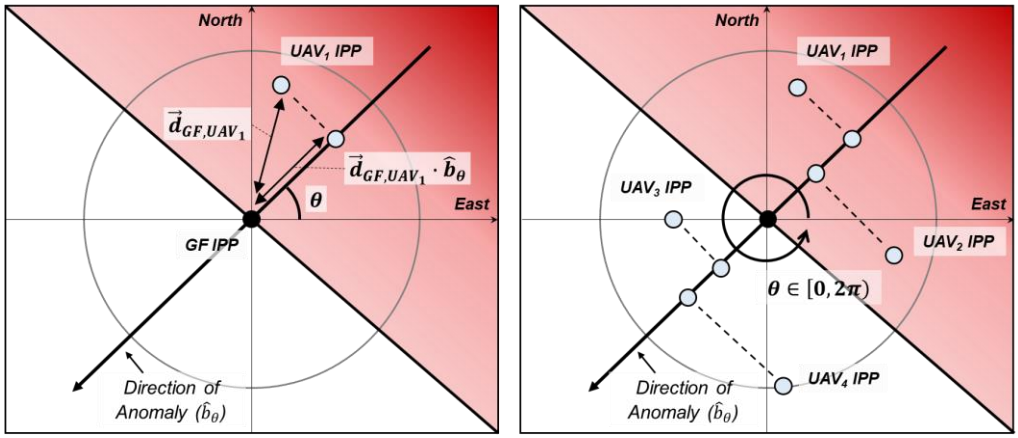

Figure 2 *IPP configuration of the ground station and a single UAV (left), and with multiple UAVs for an arbitrary direction of anomaly (right).*

4. PERFORMANCE EVALUATION OF NETWORKED IONOSPHERIC MONITORING

4.1 Simulation Results in Gradient Domain

Simulations are conducted to compute the worst undetected gradient of one satellite with randomly distributed networked UAVs. Two different distributions with randomly sampled locations of 8 UAVs within 25 km from the LADGNSS reference station are considered. Since the MDID of IGM is insensitive to the distance from the reference station, we assume the same value of MDID which is 2.83 m to compute the worst undetected gradient for each UAV.

Figure 3 shows the worst undetected gradients computed by the networked ionospheric monitoring algorithm. The outer UAVs indicated in red cannot obtain any benefit because the gradient computed for a certain anomaly direction exceeds its upper bound, 425 mm/km. For example, if UAV 4 with the closely distributed network is set as the user, other UAVs cannot protect UAV 4 against ionospheric anomalies which move from south to north. However, the inner UAVs indicated in blue obtain benefit because the outer UAVs protect the inner UAVs against all ionospheric anomaly directions. As the UAVs are more widely distributed, the outer UAVs can better protect the inner UAVs against ionospheric anomalies. Therefore, the worst undetected gradients of the inner UAVs with the widely distributed networked UAVs (the right plot of Figure 3), are smaller than those of the inner UAVs' with the closely distributed networked UAVs (the left plot of Figure 3).

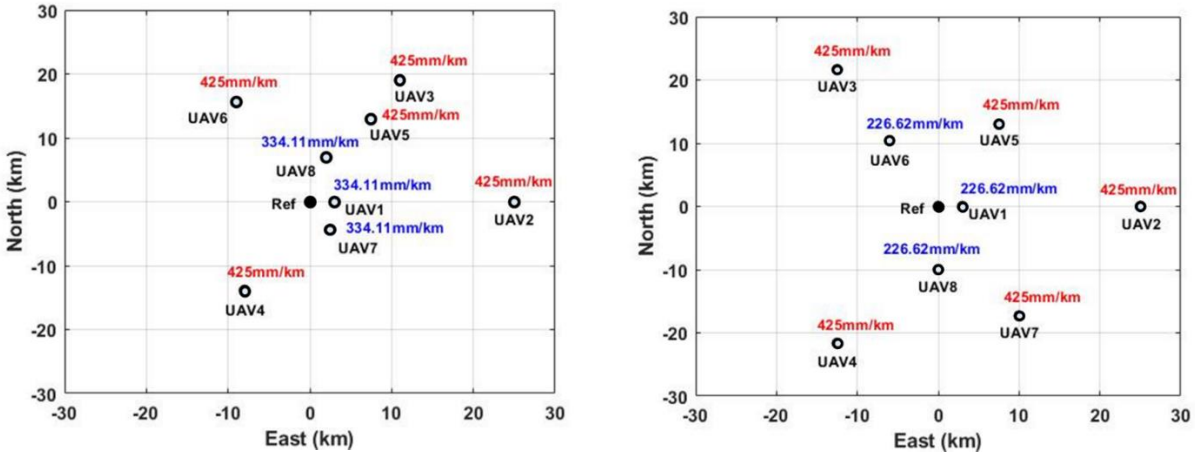

Figure 3 *The worst undetected gradients with the closely distributed networked UAVs (Left) and the widely distributed networked UAVs (Right). The UAVs indicated in red are the outer UAVs which cannot obtain any benefit from the networked UAVs and the UAVs indicated in blue are the inner UAVs which obtain benefit from the outer UAVs.*

4.2 Simulation Results in Vertical Error Domain

Based on the simulation result in the gradient domain, we conduct the simulation in the vertical error domain to evaluate the benefit of the networked ionospheric monitoring algorithm in terms of the maximum ionosphere-induced vertical error (MIEV). Among the randomly distributed UAVs in Figure 3, we choose UAV_1 as a user, which is located 3 km from the reference station. To compute MIEV, we used the two-satellite impacted hypothesis presented in Lee et al., 2011, and L5/E5a-based Divergence-Free measurement error models proposed in Nam et al., 2021. For DCDF LADGNSS measurement error models, we utilized the 27-satellite "expandable" GPS constellation almanac (GPS SPS PS, 2020) and a 27-Galileo constellation. A elevation mask angle of 10° for satellite visibility is used for both constellations. Other parameters for the error models are shown in Table 1. We conduct the simulations using the January 1, 2009 satellite geometry with an interval of 600 s between time epochs and a fixed reference station located at KAIST campus, Daejeon, South Korea.

Table 1 *Simulation parameters*

Parameter	Description	Value or Range [Unit]
τ_{gnd}	Ground Smoothing Time	30 [s] (Nam et al., 2021)
τ_{air}	Airborne Smoothing Time	30 [s] (Nam et al., 2021)
v_{air}	UAV speed	15 $[m/s]$
ρ	Correlation coefficient of ground multipath	0.1 (Nam et al., 2021)
σ_{vig}	Standard deviation of nominal ionospheric spatial gradient uncertainty	4 $[mm/km]$ (Lee et al., 2007)
σ_N	Tropospheric refractivity index uncertainty	23 (van Graas & Zhu, 2011)
h_0	Tropospheric scale height	15,730 $[m]$ (van Graas & Zhu, 2011)
$\sigma_{tropo,non\text{-}nominal}$	Bounding standard deviation for non-nominal troposphere	5 $[mm/km]$ (van Graas & Zhu, 2011)
x_{user}	Distance between the reference and user	3 [km]

The blue curves of Figure 4 shows the MIEVs of the user when benefitted from the closely (left) or widely (right) distributed networked UAVs at the KAIST campus located in Daejeon, South Korea. The MIEVs with the closely or widely distributed networked UAVs are reduced by about 0.5 m and one meter, respectively, when compared to the MIEV for the single UAV case. Therefore, this result also confirms that the benefit in the vertical error domain increases as UAVs are more widely distributed.

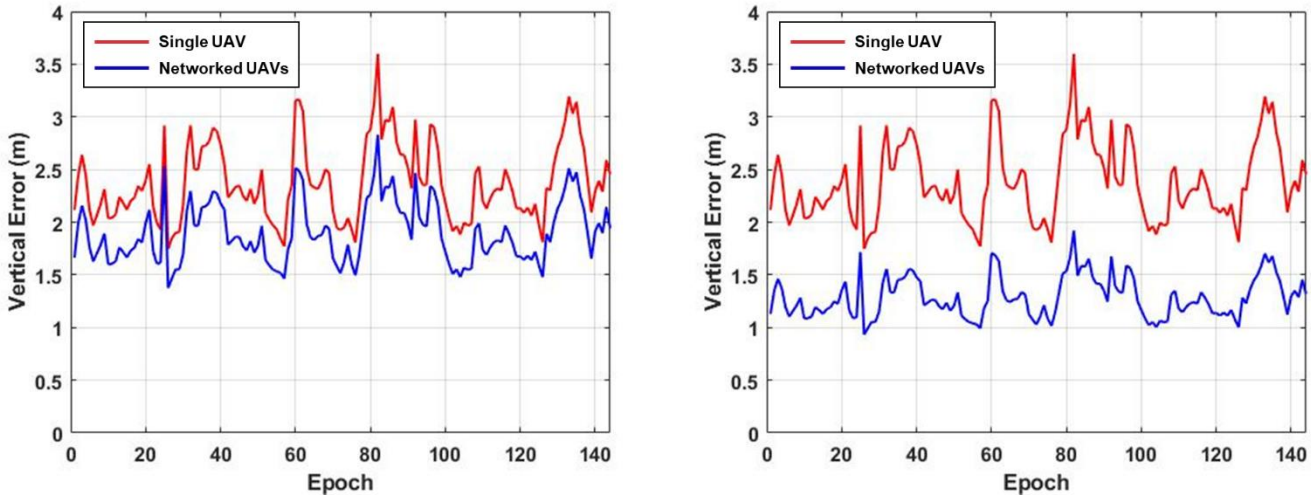

Figure 4 *MIEVs with the closely distributed networked UAVs (Left) and the widely distributed networked UAVs (Right) at the KAIST campus. The red solid curve shows the MIEV for the single UAV case, and the blue solid curve shows the MIEV with the networked UAVs.*

4.3 Sensitivity Analysis

The performance of the networked ionospheric monitoring algorithm is significantly affected by the distribution of UAVs. Thus, it is important to analyze the sensitivity of the performance to changes in the distribution of UAVs. In this study, for ideally distributed networked UAVs, we conducted sensitivity analysis by varying the distance between the reference station and networked UAVs, and the number of networked UAVs. For a fixed number of UAVs, the performance can be maximized when UAVs are most distantly and evenly distributed. Therefore, in this study, we assumed an ideal distribution for which the UAVs are located at the edge of LADGNSS coverage, and the angle between adjacent UAVs is $2\pi/N$ where N is the number of UAVs. Simulations are conducted for an ideally distributed three, four, or an infinite number of UAVs, and for a LADGNSS coverage of 25 km or 50 km. The simulation parameters are identical to those in section 4.2 and Table 1, except that the location of the user varies between 1 km to 25 km along the east axis of the reference station.

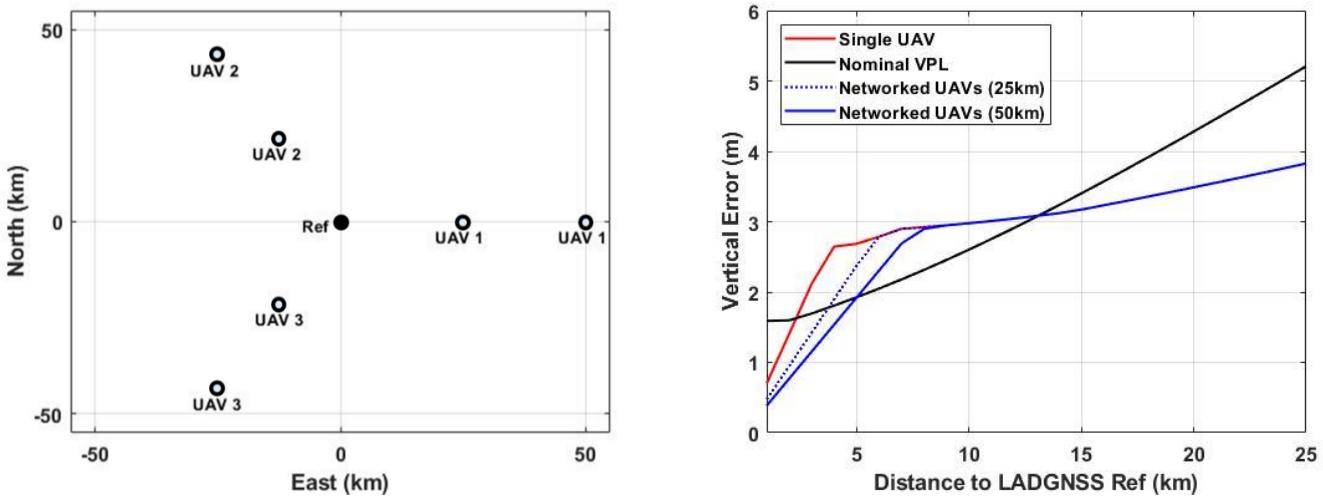

Figure 5 *The configuration of ideal triangle distributions with a coverage of 25 km or 50 km (Left) and the resulting MIEVs at a specific epoch (January 1, 2009, 00:00:00) as a function of the distance to the LADGNSS reference station (Right). The red solid curve is the MIEV for the single UAV case, the block solid curve is the nominal VPL, the blue dotted curve is the MIEV with the ideal triangle distribution with a coverage of 25 km, and the blue solid curve is the MIEV with a coverage of 50 km.*

Figure 5 shows the configuration of ideally distributed 3 UAVs located at the edge (25 km or 50 km) of the LADGNSS coverage, and the resulting MIEVs at one specific epoch (January 1, 2009, 00:00:00) as a function of distance to the reference station. The MIEVs for a single UAV and networked UAVs (25km and 50km) show rapid growth before the detection points where the ionosphere-induced differential range errors exceed MDID. Beyond these points, the user IGM starts to reliably detect the anomalous ionospheric gradient. As a result, there are transition points where the MIEVs become smaller than the nominal VPL (the black line). The IGMs of the networked UAVs distributed in regular triangles can detect ionospheric anomalies which cannot be detected by the IGM of a user. Therefore, the use of the networked UAVs reduces the MIEVs for both 25km and 50km coverage cases compared to the single UAV case. Since the IGM of a UAV farther from the reference station has a better ionospheric anomaly detection capability, the MIEV with the 50 km coverage is smaller than the MIEV with the 25 km coverage.

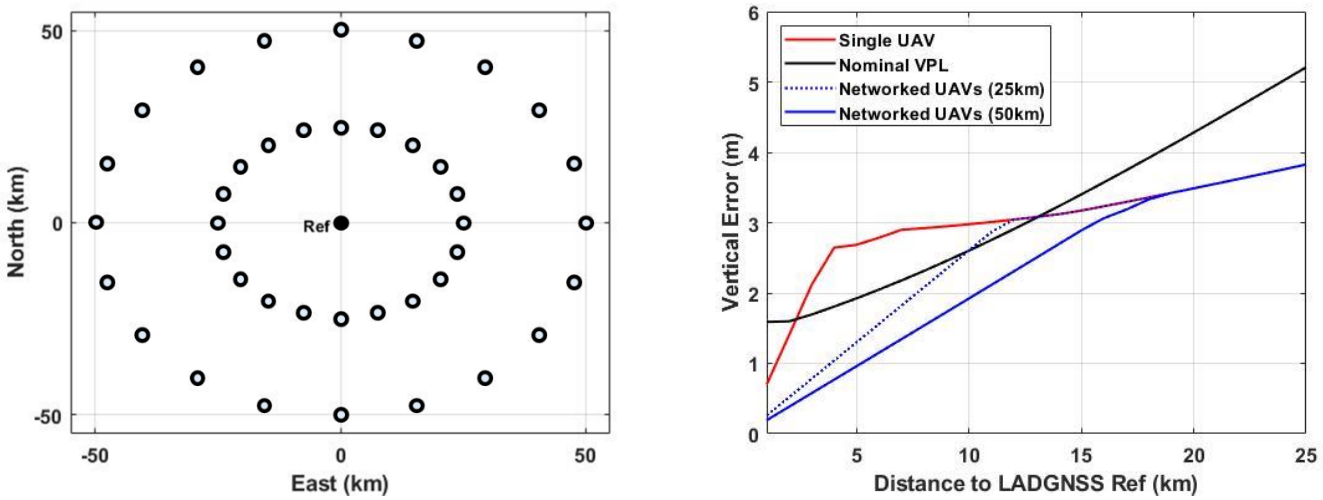

Figure 6 *The configuration of ideal circular distribution with a coverage of 25 km or 50 km (Left) and the resulting MIEVs at a specific epoch (January 1, 2009, 00:00:00) as a function of the distance to the LADGNSS reference station (Right). The red solid curve is the MIEV for the single UAV case, the block solid curve is the nominal VPL, the blue dotted curve is the MIEV with the ideal triangle distribution with a coverage of 25 km, and the blue solid curve is the MIEV with a coverage of 50 km.*

Figure 6 shows the configuration of ideal circular distributed UAVs located at the edge (25 km or 50 km) of the LADGNSS coverage, and the resulting MIEVs at one specific epoch (January 1, 2009, 00:00:00) as a function of distance to the reference station. A large but finite number of UAVs are distributed to reliably detect an ionospheric anomaly front with any direction, as shown in Figure 7. These cases show the nearly optimal performance of the networked ionospheric monitoring algorithm, and the MIEV with the 50 km coverage is reduced by about 58% on average within 10 km from the reference station, when compared to that of the single UAV case. Furthermore, the MIEV with the 50 km coverage is smaller than the nominal VPL for any distance to the reference station, and thus the ionospheric anomaly does not degrade the LADGNSS performance.

5. CONCLUSIONS

This study proposes a strategy of ionospheric gradient monitoring for DFMC LADGNSS utilizing multiple UAVs connected to the LADGNSS ground systems using two-way datalinks to enhance system performance. “Networked ionospheric monitoring” takes advantage of IGM test statistics from all UAVs supported by LADGNSS, including the one with that happens to provide the best detection capability based on its location relative to the ground station and every other UAV. In other words, every UAV has a “best other” UAV in the network that supports it by contributing the minimum value of the maximum undetected gradient among all networked UAVs. The networked monitoring algorithm computes a gradient for each UAV and all possible anomaly directions based on determining the smallest gradient that at least one UAV within the network can reliably detect.

Simulations have been conducted to evaluate the benefit of this monitoring strategy with varying configurations of networked UAVs in terms of MIEV at a typical "user" UAV location within the network. The results show significant reductions in ionospheric anomaly-induced errors by utilizing networked UAVs. As expected, the benefit of networked UAVs increases with a larger number of UAVs that are more widely distributed within the region covered by a single LADGNSS ground station. For the ideal case UAV configuration, MIEV is reduced by about 58 % compared to the single (independent or non-networked) UAV scenario.

ACKNOWLEDGMENTS
This work was supported by the National Research Foundation of Korea (NRF) grant funded by the Korea government (MSIT) (No. NRF-2019M1A3B2A04102714).

REFERENCES
Datta-Barua, S., Lee, J., Pullen, S., Luo, M., Ene, A., Qui, D., Zhang, G., & Enge, P. (2010). "Ionospheric threat parameterization for local area global-positioning-system-based aircraft landing systems." *AIAA Journal of Aircraft*, 47(4), 1141-1151. https://doi.org/10.2514/1.46719

Felux, M. (2018). *Total system performance of GBAS-based automatic landings* (Doctoral dissertation). Technical University of Munich. https://elib.dlr.de/121908/1/Felux-Michael.pdf

Global Positioning System Standard Positioning Service Performance Standard (GPS SPS PS), Washington, DC, U.S. Department of Defense, 5th Edition, April 2020. https://www.gps.gov/technical/ps/2020-SPS-performance-standard.pdf

Kim, D., Lee, J., Kim, M., Lee, J., & Pullen, S. (2017). "High-Integrity and Low-Cost Local-Area Differential GNSS Prototype for UAV Applications." *Proc. of the 30th International Technical Meeting of the Satellite Division of The Institute of Navigation (ION GNSS+ 2017)*, Portland, OR, 2031-2054. https://doi.org/10.33012/2017.15110

Lee, J., Seo, J., Park, Y. S., Pullen, S., & Enge, P. (2011). "Ionospheric threat mitigation by Geometry Screening in ground-based augmentation systems." *AIAA Journal of Aircraft*, 48(4), 1422–1433. https://doi.org/10.2514/1.c031309

Nam, G., Kim, D., Kim, N. M., Lee, J., & Pullen, S. (2021). "Enhanced Local-Area DGNSS for Autonomous Vehicle Navigation: Optimal Smoothing Strategy." *Proc. of the 34th International Technical Meeting of the Satellite Division of The Institute of Navigation (ION GNSS+ 2021)*, St. Louis, MO, 4080-4096. https://doi.org/10.33012/2021.18066

Nam, G., Min, D., Kim, N. M., Lee, J., & Pullen, S. (2022). "Optimal Smoothing and Monitor Strategies for Dual-Frequency Dual-Constellation (DFDC) LADGNSS under Anomalous Ionospheric Conditions." *Proc. of the 2022 International Technical Meeting of The Institute of Navigation*, Long Beach, CA, 1156-1174. https://doi.org/10.33012/2022.18166

Pullen, S., Enge, P., & Lee, J. (2013). "Local-Area Differential GNSS Architectures Optimized to Support Unmanned Aerial Vehicles." Proceedings of ION ITM 2013, San Diego, CA.
http://web.stanford.edu/group/scpnt/gpslab/pubs/papers/Pullen_IONITM_2013_ LADGNSSforUAVNetworksITM2013final.pdf